Dynamical generation of topological masses in Dirac fermions

Yuan-Yao He, Xiao Yan Xu, Kai Sun, Fakher F. Assaad, Zi Yang Meng, and Zhong-Yi Lu

Phys. Rev. B **97**, 081110 — Published 22 February 2018

DOI: 10.1103/PhysRevB.97.081110

Dynamical Generation of Topological Masses in Dirac Fermions

Yuan-Yao He,[1] Xiao Yan Xu,[2,3] Kai Sun,[4] Fakher F. Assaad,[5] Zi Yang Meng,[2,3] and Zhong-Yi Lu[1]

[1] *Department of Physics, Renmin University of China, Beijing 100872, China*
[2] *Beijing National Laboratory for Condensed Matter Physics, and Institute of Physics, Chinese Academy of Sciences, Beijing 100190, China*
[3] *School of Physical Sciences, University of Chinese Academy of Sciences, Beijing, 100190, China*
[4] *Physics Department, University of Michigan, Ann Arbor, MI 48109, USA*
[5] *Institut für Theoretische Physik und Astrophysik, Universität Würzburg, 97074 Würzburg, Germany*

(Dated: February 6, 2018)

We report discovery of a topological Mott insulator in strongly-correlated Dirac semimetals. Such an interaction-driven topological state has been theoretically proposed but not yet observed with unbiased large scale numerical simulations. In our model, interactions between electrons are mediated by Ising spins in a transverse field. The results indicate that the topological mass term is dynamically generated and the resulting quantum phase transition belongs to the (2+1)D $N = 8$ chiral Ising universality class. These conclusions stem from large scale sign free quantum Monte Carlo simulations.

PACS numbers: 71.10.Fd, 02.70.Ss, 05.30.Rt., 11.30.Rd

Introduction. Combination of the richness of quantum many-body effects and the elegance of topological physics[1–5] has revealed remarkable phenomena and new principles of physics, such as the fractional quantum Hall effect[6,7] and topological order[8]. Among these discoveries, one intriguing example is interaction-driven topological states, where strong correlations among particles convert a conventional state of matter into a topological one. One pathway towards such states is to utilize the phenomenon of spontaneous symmetry breaking[9–13], i.e. in a system where nontrivial topological structures are prohibited by symmetry, strong interactions can spontaneously break symmetry and thus stabilize a topologically nontrivial ground state. As proposed in Ref.[9], such a phenomenon can arise in a 2D Dirac semimetal (DSM) through a quantum phase transition that breaks spontaneously the time-reversal or the spin rotational symmetry, resulting in an interaction-driven, quantum-Hall or quantum-spin-Hall (QSH), topological insulator, dubbed topological Mott insulators (TMI)[14].

Although the general principle about TMI has been well understood, finding such a state via unbiased theoretical/numerical methods turns out to be challenging due to the strong coupling nature of the problem and the presence of competing orders. Extensive numerical efforts on interacting DSMs[15–21] report negative results, suggesting that in all explored parameter regimes, topologically-trivial competing states always have lower energy and thus the proposed TMI states cannot be stabilized. The successful alternative came lately, by substituting the DSM by a semimetal with a quadratic band crossing[10,11,22], an interaction-driven quantum Hall state is observed numerically[23]. Furthermore, experimental realization of such scenario has very recently been proposed in functionalized α-Fe_2O_3 nanosheet[24]. However, whether a TMI can emerge from a DSM without the assistance of a quadratic band crossing point, as in the original proposal[9], still remains an open question. It is also worthwhile to highlight that between the two possible types of TMIs, quantum Hall and quantum spin Hall[9], only the former has been observed in numerical studies[23]. Hence, to find a time-reversal invariant TMI is one key objective of this study.

On the other hand, in a seemingly unrelated research area, recent developments in sign-problem-free quantum Monte Carlo (QMC) approaches for itinerant fermions coupled to fluctuating bosonic fields open the door to investigate many intriguing strongly-correlated systems, such as antiferromagnetic fluctuations mediated superconductivity in metals[25,26], nematic quantum critical points in itinerant systems[27,28], as well as non-fermi liquid in itinerant quantum critical regions[29–31]. The strong-coupling nature of these systems makes analytical approach challenging[32–36], and hence sign-problem-free QMC solutions pave a new avenue towards quantitative understanding about these systems. These QMC approaches also offer a new platform for studying strongly-correlated topological states, and have recently been utilized to study topological phase transitions in DSM[37] and exotic states with topological order[38–40].

In this Letter, we study interaction-driven topological Mott insulators in Dirac semimetals with the aforementioned QMC approach. Instead of bare interactions, our model utilizes fluctuating bosonic fields to mediate interactions between fermions. At the level of the effective field theory, the model is equivalent to the originally proposed TMI model in Ref.[9], except for a minor difference in symmetry irrelevant to topology. For the study of TMI, our modified model shows two advantages: (1) other competing orders are strongly suppressed, allowing a clear TMI phase; (2) the sign-problem is avoided and thus the model can be solved via QMC techniques. Comparing to previous exact diagonalization studies[16–18,20,23], the QMC approach can access much

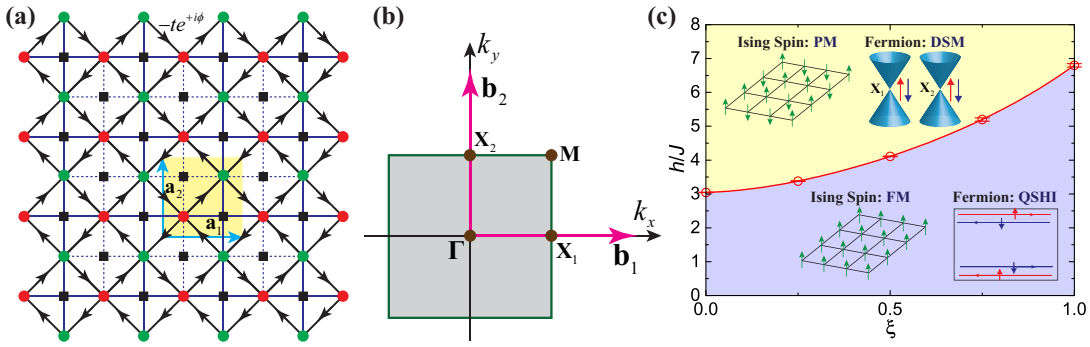

FIG. 1. The checkerboard lattice and the ground-state phase diagram. (a) The checkerboard lattice (disks) and the dual lattice (squares). Fermionic fields (Ising spins) are introduced to the lattice (dual lattice) sites. A unit cell of the lattice, indicated by $\mathbf{a}_1 = (1, 0), \mathbf{a}_2 = (0, 1)$, contains two fermion sites (A and B sublattices represented by red and green disks) and two Ising spins (black squares). (b) The Brillouin zone. For H_{Fermion}, the band structure contains two Dirac points at $\mathbf{X}_1$ and $\mathbf{X}_2$. (c) The phase diagram. Paramagnetic (PM) and ferromagnetic (FM) phases of the Ising spins are separated by a continuous phase transition, which belongs to $N = 8$ chiral Ising universality class with critical exponents $\nu = 0.85(2)$ and $\eta = 0.61(7)$ for finite ξ. At $\xi = 0$, the phase transition belongs to 3D Ising universality class. In the PM (FM) phase, fermions form a Dirac semimetal (quantum spin Hall insulator)

larger system size and reveals detailed information about the critical properties associated with the interaction-driven topological transition. Our QMC results show a continuous quantum phase transition from a DSM state to a QSH-type TMI phase, with the critical scaling at the quantum critical point agreeing nicely with the $N = 8$ chiral Ising universality[41,42].

Model and Method. Our model describes Dirac fermions coupled to a transverse field Ising model. As illustrated in Fig. 1(a), fermions in this model reside on the lattice sites (disks), while Ising spins are placed on each dual lattice site (squares) at the plaquette centers. The Hamiltonian consists of three parts,

$$H = H_{\text{Fermion}} + H_{\text{Ising}} + H_{\text{Coupling}}, \quad (1)$$

$$H_{\text{Fermion}} = -t \sum_{\langle ij\rangle\sigma} (e^{+i\sigma\phi} c^\dagger_{i\sigma} c_{j\sigma} + e^{-i\sigma\phi} c^\dagger_{j\sigma} c_{i\sigma}),$$

$$H_{\text{Ising}} = -J \sum_{\langle pq\rangle} s^z_p s^z_q - h \sum_p s^x_p,$$

$$H_{\text{Coupling}} = \sum_{\langle\langle ij\rangle\rangle\sigma} \xi_{ij} s^z_p (c^\dagger_{i\sigma} c_{j\sigma} + c^\dagger_{j\sigma} c_{i\sigma}).$$

where indices i, j represent fermion sites and p, q label the dual lattice sites for Ising spins s^z. Fermion spins are labeled by subindex σ. H_{Fermion} describes the nearest-neighbor (NN) hopping for fermions, which contains a staggered flux $\pm 4\phi$ for each plaquette. Here, we request spin-up and spin-down fermions to carrier opposite flux patterns to preserve the time-reversal symmetry. The Ising spins are governed by H_{Ising}, which describes a ferromagnetic ($J > 0$) transverse-field Ising model[43–45]. The last term H_{Coupling} couples the Ising spins with the next-nearest-neighbor (NNN) fermion hoppings, where the coupling constant $\xi_{ij} = \pm\xi t$ has a staggered sign structure alternating between neighboring plaquette, i.e., $+$ $(-)$ for solid (dashed) NNN bonds as illustrated in Fig. 1(a). Up to a basis change, the low-energy physics in this model can be described by the following effective field theory $S = \sum_\sigma \int \mathbf{dr} dt \bar{\Psi}_\sigma (i\gamma^\mu \partial_\mu + g\sigma\varphi\gamma^3\gamma^5)\Psi_\sigma + S_\varphi$, where γ^μ are gamma matrices and φ is a bosonic field governed by the φ^4-theory S_φ. Here, $\sigma = \pm 1$ (up or down) is the fermion spin index, and g is the coupling constant for the boson-fermion interactions. This effective field theory is in strong analogy to the model proposed early on in Ref.[9], provided that we decouple the fermion-fermion interactions with a Hubbard-Stratonovich auxiliary field, as appropriate in the limit $h/J \to \infty$[38]. It is also worthwhile to emphasize that in our model, the fermion spins only preserve U(1) symmetry, while the model in Ref.[9] has a SU(2) spin symmetry. This difference has little effect on topological properties, but as discussed below it changes the critical scaling as well as the finite temperature phase diagram.

As in the original model of TMI, our Hamiltonian also contains a symmetry which prohibits nontrivial topology. It is easy to verify that our Hamiltonian is invariant under the following Z_2 transformation, $\hat{P} = \hat{R}_x(\pi) \times \hat{T}_{A\to B}$, where $\hat{R}_x(\pi)$ stands for π-rotation along x-axis for both Ising and fermion spins, and $\hat{T}_{A\to B}$ represents space translation from sublattice A to B inside a unit cell. Because the topological index (the spin Chern number) flips sign under this transformation, this symmetry requires the index to vanish and thus any (quantum spin Hall) topological insulator is prohibited, unless this Z_2 symmetry is broken spontaneously.

To explore the ground-state phase diagram of this model, we employ the projector quantum Monte Carlo (PQMC) method[46], with details presented in Sec.I.A of the supplemental material (SM)[47]. In addition to the usual local updates of Ising spins, both Wolff[48] and geometric cluster updates[49] are applied in our simulations,

as shown in Sec.I.B of SM[47]. Our QMC simulations are free of the sign problem at and away from half filling[50]. In this Letter, we focus on the coupling strength $0 \leq \xi \leq 1$ with $J = t = 1$ and the system sizes simulated in this work are $L = 4, 6, 8, 10, 12, 14$ with $N = L^2$ unit cells and $N_s = 2L^2$ lattice sites.

Ground state phase diagram. The ground state phase diagram in the $\xi - h$ plane is shown in Fig. 1(c). Several regimes in the phase diagram can be solved exactly. At $\xi = 0$, the fermions and Ising spins decouple: the fermions form a non-interacting Dirac semimetal, and the Ising spins undergo a paramagnetic to ferromagnetic (PM-FM) quantum phase transition at $h_c = 3.046(3)$ in the 3D Ising universality class[37,51,52]. At $h = 0$, quantum fluctuations of Ising spins vanish and Ising spins form a fully-polarized FM state. As a result, the fermions turn into a non-interacting quantum-spin-Hall topological insulator, whose Hamiltonian is $H_{\text{Fermion}} + H_{\text{Coupling}}$ with fully polarized Ising spins $s^z = +1(-1)$ [10,23,53] (See Sec. V.A in the SM[47] for details). At $h \to \infty$, the Ising spins are aligned along the x-axis. Second order perturbation theory around this point, gives rise to an interaction of order ξ^2/h between the fermions. Since the Dirac semimetal is a stable state of matter, we expect that it will be realized in the limit $h \to \infty$.

At $\xi > 0$ and intermediate h, we find a direct second-order quantum transition between the PM and FM phases. This transition is also the topological phase transition for the fermions, in which the Dirac semimetal acquires a topological mass gap corresponding to the quantum spin Hall topological insulator. This conclusion is consistent with the symmetry analysis above, where the PM (FM) phase preserve (spontaneously breaks) the Z_2 symmetry and thus a quantum spin Hall insulator is prohibited (allowed). At $\xi > 0$, the scaling exponents at the transition deviates from the 3D Ising universality class. Due to the coupling between fermions and bosons, the $\xi > 0$ phase transition flows to a different universality class, namely the $N = 8$ component chiral Ising universality class[41,42].

FM-PM phase transition for Ising spins. We determine the location of QCP via the Binder cumulant[54]: $U_2 = \frac{1}{2}(3 - \frac{\langle m^4 \rangle}{\langle m^2 \rangle^2})$ and correlation ratio[55,56]: $R_{\text{Corr}} = 1 - \frac{S^{\text{Ising}}(\mathbf{Q}+\mathbf{q})}{S^{\text{Ising}}(\mathbf{Q})}$, where $m = \frac{1}{N_s}\sum_p s_p^z$ and $S^{\text{Ising}}(\mathbf{k})$ is the trace of the structure factor matrix (2×2) of Ising magnetic order at $\mathbf{k}$ point. Here, $\mathbf{Q} = \mathbf{\Gamma} = (0, 0)$ is the ordering vector for Ising spin, and $\mathbf{q}$ is the smallest momentum on the lattice, i.e., $(0, \frac{2\pi}{L})$ or $(\frac{2\pi}{L}, 0)$. Both U_2 and R_{Corr} converge to 0 (1) in the PM (FM) phase at the thermodynamic limit. The crossing points for finite-size results of U_2 and R_{Corr}, respectively, provide the location of QCP. In this way, we first determine the position of QCP and then perform finite-size scaling analysis of $\langle m^2 \rangle$ close to it to extract the critical exponents.

The results of U_2 and R_{Corr}, as well as the data collapse of $\langle m^2 \rangle$ for $\xi = 0.5$ and $\phi = \pi/4$ (π-flux in each plaquette) are presented in Fig. 2. Up to system size

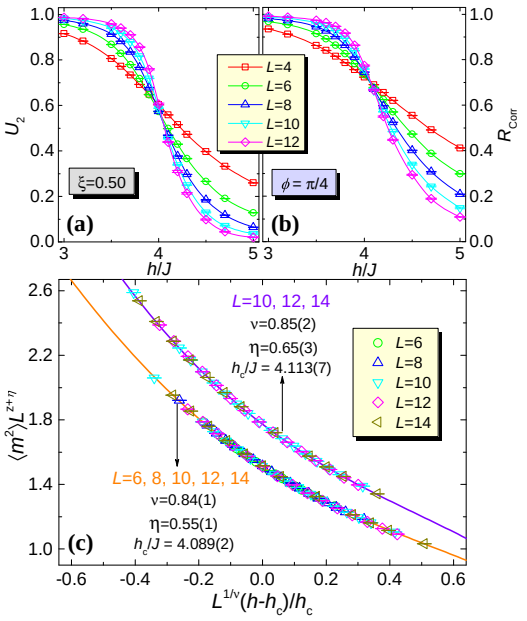

FIG. 2. (a) Binder cumulant U_2 and (b) correlation ratio R_{Corr} for $\xi = 0.50$ and $\phi = \pi/4$. (c) The data collapses of $\langle m^2 \rangle$ for $L = 6, 8, 10, 12, 14$ and $L = 10, 12, 14$, respectively. The critical exponents are also shown in (c).

$L = 12$, we can obtain the finite size crossing points $h = 4.06$ for U_2 and $h = 4.10$ for R_{Corr} as the approximate location of QCP. In Fig. 2(c), we collapse the data as $\langle m^2 \rangle L^{z+\eta} = f(L^{1/\nu}(h - h_c)/h_c)$ for $L = 6, 8, 10, 12, 14$ and $L = 10, 12, 14$, respectively. The critical exponents extracted from these two collapses are slightly different especially in η, indicating some finite-size effect. As will be discussed below, this shifting of exponents is due to a crossover phenomenon. Combining both collapses, we take the exponents as $\nu = 0.85(2), \eta = 0.61(7)$ (taking $z = 1$) with $h_c = 4.11(1)$, which are well consistent with the results presented in Ref.[41] as $\nu = 0.83(1), \eta = 0.62(1)$ for $N = 8$ components chiral Ising universality class.

We employed two additional measurements to further corroborate the critical exponents. First, we performed finite-size scaling analysis for $S^{\text{Ising}}(\mathbf{k})$ at $\xi = 0.50$ and $\phi = \pi/4$, which is shown in Sec. II.B of the SM[47], with the extracted critical exponents $\nu = 0.84(4), \eta = 0.62(6)$. Second, we also simulated the model with $\xi = 0.50$ and $\phi = \pi/8$ (half-π flux) and obtained the critical exponents from the finite-size scaling of $\langle m^2 \rangle$, and the results are presented in Sec. III.A of SM[47]. The obtained critical exponents are $\nu = 0.85(3), \eta = 0.63(7)$ with $h_c = 4.242(3)$. These exponents are well consistent with those in Fig. 2(c), rendering the $N = 8$ components chiral Ising universality class.

The properties of QCPs for the PM-FM phase transitions of Ising spins for $\xi = 0.25, 0.75, 1.00$ as presented in the phase diagram of Fig. 1(c), are also determined with U_2 and R_{Corr}, as well as the finite-size scaling of $\langle m^2 \rangle$ and excitation gaps of fermions.

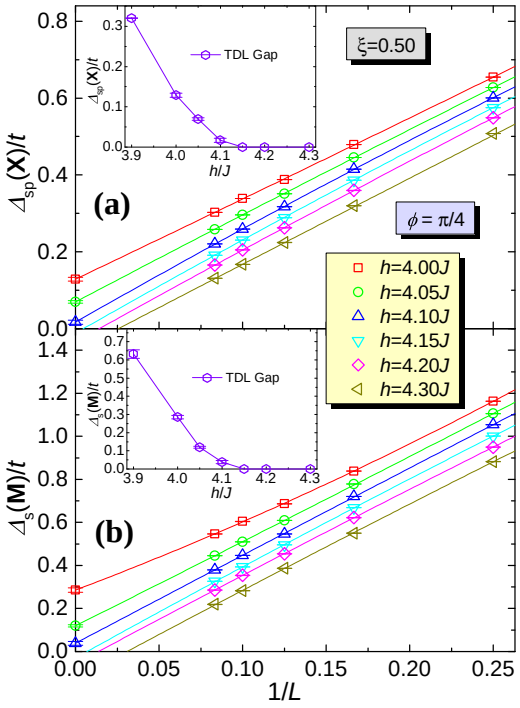

FIG. 3. (a) The single-particle gap $\Delta_{sp}(\mathbf{X})$ and (b) the spin gap $\Delta_s(\mathbf{M})$ close to the QCP $h_c = 4.11(1)$ for $\xi = 0.50$ and $\phi = \pi/4$. The insets are the excitation gaps at thermodynamic from the extrapolation with second-order polynomials in $1/L$. Both single-particle and spin gaps open at $h/J = 4.10 \sim 4.15$, consistent with QCP of PM-FM phase transition of Ising spins.

Topological phase transition for fermions. Our numerical results further show a single phase transition from Dirac semimetal to topological Mott insulator with decreasing transverse-field h, which comes hand in hand with the PM-FM phase transition of Ising spins. As shown in Fig. 3, we find that the fermions remains gapless in the PM phase with vanishing gap at the Dirac point. Here, both $\Delta_{sp}(\mathbf{X})$, the average single particle gap at two Dirac points $\mathbf{X}_1$ and $\mathbf{X}_2$, and $\Delta_s(\mathbf{M})$, the two-particle spin gap at M, vanish at the thermodynamic limit, consistent with the Dirac semimetal spectrum. In the FM phase, both gaps start to merge at $h/J = 4.10 \sim 4.15$, consistent with the location of PM-FM phase transition point for Ising spins. It is worthwhile to highlight that the gaps remain finite in the whole FM phase with $h < h_c$, indicating the absence of topological phase transition. Since the fermions form a quantum spin Hall insulator in the exactly solvable limit at $h = 0$, this finite gap implies that the whole FM phase shares the same nontrivial topology. To further verify this conclusion, we compute directly the topological invariant[57], the spin Chern number $C_s = (C_\uparrow - C_\downarrow)/2$. As shown in Sec. V.B. of SM[47], we obtain $C_s = +1$ for whole $h < h_c$ region, indicating that FM phase is a quantum-spin-Hall topological insulator.

In Sec. IV of SM[47], we present raw data of dynamic quantities $G(\mathbf{k}, \tau)$ and $S^{xy}(\mathbf{k}, \tau)$, from which $\Delta_{sp}(\mathbf{X})$ and $\Delta_s(\mathbf{M})$ are extrapolated. The comparisons between $2\Delta_{sp}(\mathbf{X})$ and $\Delta_s(\mathbf{M})$ are also shown to reveal the effect of electron-electron interactions. Furthermore, the gap opening of $\Delta_{sp}(\mathbf{X})$ and $\Delta_s(\mathbf{M})$ at $\xi = 0.25, 0.75, 1.00$ match the QCPs of PM-FM phase transition for Ising spins, thus supporting the picture of a semimetal-TMI topological phase transition.

Finite-size scaling crossover. As discussed above at $\xi = 0$ and $\xi > 0$, the PM-FM transition belongs to two different universality classes, 3D Ising and $N = 8$ chiral Ising. As a result, in the thermodynamic limit, the scaling exponents will change discontinuously as we change the value of ξ away from 0. In numerical studies, because of the finite size, such a discontinuous change will not show up. Instead, a crossover behavior is expected, i.e. at small ξ, a crossover length scale $L_c(\xi)$ shall arise. For $L < L_c$ ($L > L_c$), the scaling behavior merges towards the 3D Ising ($N = 8$ chiral Ising) universality class. As ξ approaches zero (increases), L_c diverge to infinity (decreases to microscopic values) and thus the 3D Ising ($N = 8$ chiral Ising) universality class is fully recovered. Such an effect is indeed observed in our data. In Sec. VI in SM[47], we present the finite-size scalings of $\langle m^2 \rangle$ from $L = 6, 8, 10, 12$ and $L = 8, 10, 12$, respectively, for $\xi = 0.25, 0.50, 0.75$. At $\xi = 0.25$, the data collapse suffers strongly from the finite-size effect, and chiral Ising exponents only arise in very large system sizes, especially for η. However, as ξ increases, the chiral Ising exponents emerge even if the smallest size $L = 6$ is included in the fitting.

Discussions. Because the fermion spin in our model only preserves a $U(1)$ symmetry, instead of $SU(2)$, our topological Mott insulator breaks a Z_2 symmetry in contrast to the $SU(2)$ symmetry breaking in Ref.[9]. This difference in symmetry breaking patterns is irrelevant for topology. However, this leads to different scaling exponents at the transition[41]. Furthermore, at finite temperature, the symmetry breaking phase in our model survives, while the $SU(2)$ symmetry breaking arises only at $T = 0$.

To the best of our knowledge, our study demonstrates the first interaction-driven quantum-spin-Hall topological Mott insulator from unbiased numerical method, and for the first time, this novel topological phenomenon becomes accessible to large-scale lattice QMC simulations. Our work points out a new route to realize interaction-driven topological phases and phase transitions. It has experimental relevance since the interaction-driven quantum anomalous Hall effect has recently being suggested in functionalized α-Fe_2O_3 nanosheet[24].

We (YYH, XYX, ZYM and ZYL) acknowledge fundings from the Ministry of Science and Technology of China through National Key Research and Development Program under Grant No. 2016YFA0300502 and from the National Science Foundation of China under Grant Nos. 91421304, 11421092, 11474356, 11574359, 11674370 as well as the National Thousand-Young Talents Program of China. Y.Y.H is also supported by the Outstanding

Innovative Talents Cultivation Funded Programs 2016 of Renmin University of China. K.S. acknowledges support from the National Science Foundation under Grant No. PHY1402971 and the Alfred P. Sloan Foundation. F.F.A thanks the German Research Foundation (DFG) for financial support through the SFB 1170 ToCoTronics. We thank the Physical Laboratory of High Performance Computing in Renmin University of China, the Center for Quantum Simulation Sciences in the Institute of Physics, Chinese Academy of Sciences and the Tianhe-1A platform at the National Supercomputer Center in Tianjin for their technical support and generous allocation of CPU time.

[1] K. v. Klitzing, G. Dorda, and M. Pepper, Phys. Rev. Lett. **45**, 494 (1980).
[2] D. J. Thouless, M. Kohmoto, M. P. Nightingale, and M. den Nijs, Phys. Rev. Lett. **49**, 405 (1982).
[3] F. D. M. Haldane, Phys. Rev. Lett. **61**, 2015 (1988).
[4] M. Z. Hasan and C. L. Kane, Rev. Mod. Phys. **82**, 3045 (2010).
[5] X.-L. Qi and S.-C. Zhang, Rev. Mod. Phys. **83**, 1057 (2011).
[6] D. C. Tsui, H. L. Stormer, and A. C. Gossard, Phys. Rev. Lett. **48**, 1559 (1982).
[7] R. B. Laughlin, Phys. Rev. Lett. **50**, 1395 (1983).
[8] X. G. WEN, International Journal of Modern Physics B **04**, 239 (1990).
[9] S. Raghu, X.-L. Qi, C. Honerkamp, and S.-C. Zhang, Phys. Rev. Lett. **100**, 156401 (2008).
[10] K. Sun, H. Yao, E. Fradkin, and S. A. Kivelson, Phys. Rev. Lett. **103**, 046811 (2009).
[11] I. F. Herbut and L. Janssen, Phys. Rev. Lett. **113**, 106401 (2014).
[12] Y. Zhang, Y. Ran, and A. Vishwanath, Phys. Rev. B **79**, 245331 (2009).
[13] R. Yu, W. Zhang, H.-J. Zhang, S.-C. Zhang, X. Dai, and Z. Fang, Science **329**, 61 (2010), http://science.sciencemag.org/content/329/5987/61.full.pdf.
[14] We want to emphasize that here we have adopted the definition of TMI in the sense of Ref.[9], we are aware of another definition stemmed from the paper *Nature Physics* **6**, 376 (2010) , which is highly influential, equally interesting and important, but it is not within the scope of this Letter.
[15] Y. Jia, H. Guo, Z. Chen, S.-Q. Shen, and S. Feng, Phys. Rev. B **88**, 075101 (2013).
[16] N. A. García-Martínez, A. G. Grushin, T. Neupert, B. Valenzuela, and E. V. Castro, Phys. Rev. B **88**, 245123 (2013).
[17] M. Daghofer and M. Hohenadler, Phys. Rev. B **89**, 035103 (2014).
[18] H. Guo and Y. Jia, Journal of Physics: Condensed Matter **26**, 475601 (2014).
[19] J. Motruk, A. G. Grushin, F. de Juan, and F. Pollmann, Phys. Rev. B **92**, 085147 (2015).
[20] S. Capponi and A. M. Läuchli, Phys. Rev. B **92**, 085146 (2015).
[21] D. D. Scherer, M. M. Scherer, and C. Honerkamp, Phys. Rev. B **92**, 155137 (2015).
[22] K. Sun, W. V. Liu, A. Hemmerich, and S. Das Sarma, Nat. Phys. **8**, 67 (2012).
[23] H.-Q. Wu, Y.-Y. He, C. Fang, Z. Y. Meng, and Z.-Y. Lu, Phys. Rev. Lett. **117**, 066403 (2016).
[24] Q.-F. Liang, J. Zhou, R. Yu, X. Wang, and H. Weng, ArXiv e-prints (2017), arXiv:1705.00254 [cond-mat.mes-hall].
[25] E. Berg, M. A. Metlitski, and S. Sachdev, Science **338**, 1606 (2012).
[26] Y. Schattner, M. H. Gerlach, S. Trebst, and E. Berg, Phys. Rev. Lett. **117**, 097002 (2016).
[27] S. Lederer, Y. Schattner, E. Berg, and S. A. Kivelson, Phys. Rev. Lett. **114**, 097001 (2015).
[28] Y. Schattner, S. Lederer, S. A. Kivelson, and E. Berg, Phys. Rev. X **6**, 031028 (2016).
[29] X. Wang, Y. Schattner, E. Berg, and R. M. Fernandes, Phys. Rev. B **95**, 174520 (2017).
[30] S. Lederer, Y. Schattner, E. Berg, and S. A. Kivelson, Proceedings of the National Academy of Sciences **114**, 4905 (2017), http://www.pnas.org/content/114/19/4905.full.pdf.
[31] X. Y. Xu, K. Sun, Y. Schattner, E. Berg, and Z. Y. Meng, Phys. Rev. X **7**, 031058 (2017).
[32] S.-S. Lee, Phys. Rev. B **80**, 165102 (2009).
[33] M. A. Metlitski and S. Sachdev, Phys. Rev. B **82**, 075127 (2010).
[34] M. A. Metlitski and S. Sachdev, Phys. Rev. B **82**, 075128 (2010).
[35] D. Dalidovich and S.-S. Lee, Phys. Rev. B **88**, 245106 (2013).
[36] A. Schlief, P. Lunts, and S.-S. Lee, Phys. Rev. X **7**, 021010 (2017).
[37] X. Y. Xu, K. S. D. Beach, K. Sun, F. F. Assaad, and Z. Y. Meng, Phys. Rev. B **95**, 085110 (2017).
[38] F. F. Assaad and T. Grover, Phys. Rev. X **6**, 041049 (2016).
[39] S. Sachdev, E. Berg, S. Chatterjee, and Y. Schattner, Phys. Rev. B **94**, 115147 (2016).
[40] S. Gazit, M. Randeria, and A. Vishwanath, Nat Phys **13**, 484 (2017).
[41] S. Chandrasekharan and A. Li, Phys. Rev. D **88**, 021701 (2013).
[42] Y. Otsuka, S. Yunoki, and S. Sorella, Phys. Rev. X **6**, 011029 (2016).
[43] S. V. Isakov and R. Moessner, Phys. Rev. B **68**, 104409 (2003).
[44] H. W. J. Blöte and Y. Deng, Phys. Rev. E **66**, 066110 (2002).
[45] Y.-C. Wang, Y. Qi, S. Chen, and Z. Y. Meng, Phys. Rev. B **96**, 115160 (2017).
[46] F. Assaad and H. Evertz, in Computational Many-Particle Physics, Lecture Notes in Physics, Vol. 739, edited by H. Fehske, R. Schneider, and A. Weiße (Springer Berlin Heidelberg, 2008) pp. 277–356.
[47] See Supplemental Material at http://link.aps.org/supplemental/xxx for discussions on the implemention of QMC algorithm for the fermion-Ising spin coupling model, the criticality analysis, raw

data of dynamic correlation functions and analysis of topological properties of model..
[48] U. Wolff, Phys. Rev. Lett. **62**, 361 (1989).
[49] J. R. Heringa and H. W. J. Blöte, Phys. Rev. E **57**, 4976 (1998).
[50] C. Wu and S.-C. Zhang, Phys. Rev. B **71**, 155115 (2005).
[51] P. Pfeuty and R. J. Elliott, Journal of Physics C: Solid State Physics **4**, 2370 (1971).
[52] M. Hasenbusch, K. Pinn, and S. Vinti, Phys. Rev. B **59**, 11471 (1999).
[53] J.-M. Hou, Phys. Rev. Lett. **111**, 130403 (2013).
[54] K. Binder, Zeitschrift für Physik B Condensed Matter **43**, 119 (1981).
[55] R. K. Kaul, Phys. Rev. Lett. **115**, 157202 (2015).
[56] S. Pujari, T. C. Lang, G. Murthy, and R. K. Kaul, Phys. Rev. Lett. **117**, 086404 (2016).
[57] Y.-Y. He, H.-Q. Wu, Z. Y. Meng, and Z.-Y. Lu, Phys. Rev. B **93**, 195163 (2016).